

Constraints on interacting dark energy models from SDSS galaxy-galaxy weak lensing measurements

Jiajun Zhang*,¹ Rui An†,^{1,2} Wentao Luo,^{1,3} Zhaozhou Li,¹ Shihong Liao,⁴ and Bin Wang ‡^{5,1}

¹*Department of Astronomy, School of Physics and Astronomy,
Shanghai Jiao Tong University, Shanghai, 200240, China*

²*IFSA Collaborative Innovation Center, Shanghai Jiao Tong University, Shanghai, China*

³*Kavli Institute for the Physics and Mathematics of the Universe (Kavli IPMU, WPI),
Tokyo Institutes for Advanced Study, The University of Tokyo, Chiba, 277-8582, Japan*

⁴*Key Laboratory for Computational Astrophysics, National Astronomical Observatories,
Chinese Academy of Sciences, Beijing, 100012, China*

⁵*Center for Gravitation and Cosmology, College of Physical Science
and Technology, Yangzhou University, Yangzhou, 225009, China*

(Dated: March 30, 2022)

We develop a fully self-consistent N-body simulation pipeline and apply this pipeline to refine general phenomenological interacting dark energy models. Comparing our simulation results with the SDSS galaxy-galaxy weak lensing measurements, we obtain up to 820% improvement of the constraint on the interaction strength compared with the previous linear examination. This improvement attributes to the correct treatment of the non-linear structure formation at low redshifts, where weak lensing measurements are sensitive.

PACS numbers:

INTRODUCTION

The “double dark” phenomenon, dark matter and dark energy, is widely accepted in explaining various astronomical observations, such as the cosmic microwave background[1], Type Ia supernovae[2–4], galaxy rotation curves[5–7] etc. However, the nature of these dark sectors remains unknown. In the standard Λ CDM model, dark energy, which is assumed as the cosmological constant, and dark matter, which is treated as collisionless particles, are considered co-existing independently in the universe. From the field theory point of view, it is natural to ask whether there are some interactions between these two biggest components of the universe. In fact, interacting dark energy (IDE hereafter for short) models have the potential to alleviate the coincidence problem and some observational tensions suffered by the standard Λ CDM model, see [8] for a recent review and references therein.

The influence of IDE models on the background dynamics and the linear perturbation evolutions in the

universe has been studied extensively, see the review [8] and its quoted literatures. However, in the nonlinear regime the effect of interactions between dark sectors on the structure formation still remains unclear. Explanation of the nonlinear structure formation heavily relies on the numerical simulation. A preliminary attempt on the N-body simulation by considering quintessence dark energy specifically interacting with dark matter was proposed in [9, 10], where the initial condition in the simulation was naively taken from the Λ CDM model and the dark energy perturbation was not consistently computed at different scales and redshifts. For general phenomenological IDE models, self-consistent N-body simulations are still lacking. In order to examine the influence of IDE models on the structure formation at small scales, an ad-hoc halofit model[11] was borrowed in the study of nonlinear correction[12]. Given that the halofit model is the empirical fit from the Λ CDM framework, whether it can reflect the real physics of the interaction between dark sectors is a question to be answered.

In this Letter, we devise a novel cosmological N-body simulation pipeline for general phenomenological IDE models, and try to explore the physics in the structure formation when there is interaction between dark sectors. We do not limit the dark energy to be in the quintessence region, and employ the general phenomeno-

*liamzhang@sjtu.edu.cn

†an_rui@sjtu.edu.cn

‡wangb@yzu.edu.cn

logical interaction forms discussed in the market. In our simulations, we input initial parameters obtained from combined constraints for IDE models including Planck, Type Ia supernovae, baryon acoustic oscillations and the Hubble constant datasets. We include dark energy perturbations intrinsically by solving its density and velocity equations as scale and redshift dependent. Our pipeline is fully self-consistent and enough accurate in studying IDE models. We disclose that for some IDE models, naively adopting the halofit model cannot reflect real physics in the nonlinear perturbation level.

With this self-consistent and effective pipeline, we can study nonlinear structure formation at low redshifts precisely in IDE models. This enables us to employ a new probe, weak lensing, to put further constraints on IDE models. Weak lensing has been proved as a powerful tool in studying large-scale structures and halo properties at low redshifts. By measuring the shape change of the background galaxy images due to the gravitational lensing from the foreground gravitational potential, the information of the structures can be obtained. Recently, galaxy-galaxy weak lensing measurements using the SDSS data have been successfully used to study the host halo properties of galaxy groups[13, 14]. Here, we compare our simulation results with the galaxy-galaxy weak lensing measurements using the SDSS data, and find that the improvement of the constraint for the interaction strength in some IDE models can reach up to 820%. This shows the powerfulness of our cosmological N-body simulation pipeline in studying IDE models. With this tool, we can refine IDE models allowed by linear constraints[15].

PHENOMENOLOGICAL MODELS

The interaction between dark sectors is well motivated from field theory and is widely discussed in literatures, see recent review [8]. With the interaction between dark sectors, the background continuity equations of dark matter and dark energy obey

$$\dot{\rho}_c + 3H\rho_c = Q, \dot{\rho}_d + 3H(1 + w_d)\rho_d = -Q. \quad (1)$$

Here we focus on the commonly assumed phenomenological interaction form $Q = 3\xi_1 H\rho_c + 3\xi_2 H\rho_d$, where ρ_c is the dark matter density, ρ_d is the dark energy density and the dot denotes the derivative with respect to the conformal time, H is the Hubble parameter and $w_d = p_d/\rho_d$ is the equation of state for dark energy. We do not limit dark energy to be a quintessence field with $w_d > -1$ [16],

but instead allow w_d to be a free value either in the quintessence or the phantom regions. ξ_1 and ξ_2 indicate the strength of interactions.

The linear evolutions of density and velocity perturbations for dark matter and dark energy were described in [17–19]. In the subhorizon approximation, from linear level equations we can obtain the Poisson equation in the real space

$$\nabla^2 \Psi = -\frac{3}{2}H^2[\Omega_c \Delta_c + (1 - \Omega_c)\Delta_d], \quad (2)$$

where Δ_d (Δ_c) is the density perturbation of dark energy (matter), and Ω_c is the background density ratio of dark matter. It is clear that with the interaction, the gravitational potential is modified. The corresponding Euler equation in the real space reads

$$\nabla v_c + [H + 3H(\xi_1 + \frac{\xi_2}{r})]\nabla v_c = \nabla^2 \Psi, \quad (3)$$

where $r = \rho_c/\rho_d$. The coupling between dark sectors introduces an additional acceleration on dark matter particles at each time step in the simulation. In the following we will concentrate our discussions on phenomenological IDE models listed in Tab. I [15], which are natural Taylor expansions of the interaction kernel Q into energy densities ρ_c and ρ_d .

TABLE I: Phenomenological IDE models

Model	Q	w
I	$3\xi_2 H\rho_d$	$-1 < w_d < -1/3$
II	$3\xi_2 H\rho_d$	$w_d < -1$
III	$3\xi_1 H\rho_c$	$w_d < -1$
IV	$3\xi H(\rho_c + \rho_d)$	$w_d < -1$

With Planck 2015, Type Ia supernovae, baryon acoustic oscillations, and the Hubble constant observation, tight constraints on ξ_1 for Model III and ξ for Model IV were obtained in [15]. However, for Models I and II, the obtained constraints on the strengths of couplings are loose [15]. This is well expected because in Models I and II, the interaction is proportional to the energy density of dark energy, which was sub-dominant when CMB was produced. It is more reasonable to expect that the observations at low redshifts shall provide tighter constraints on Models I and II, especially the small-scale structure information. For this purpose we resort to using N-body simulations to make accurate analysis.

SIMULATION PIPELINE

Since IDE models are different from the Λ CDM model in every relevant equation, it is naive to count on empirical fits to the Λ CDM model, e.g. the halofit, to understand the physics in the nonlinear structure formation. We require a new N-body simulation pipeline to understand the structure developed in IDE models. There are four modifications we have considered in devising the new pipeline compared to the standard Λ CDM model. Firstly, the pre-initial condition is generated by the Capacity Constrained Voronoi Tessellation (CCVT) method[20], instead of the classically used glass or grid. This makes sure that our pre-initial condition is free of Poisson equation at all, generating geometrically equilibrium state of particle distribution. We have tested that using CCVT, grid or glass makes negligible differences for the pre-initial condition in simulations. The choice of CCVT is mainly because of self-consistency consideration, rather than the accuracy consideration. Secondly, the initial matter power spectrum is generated by our modified CAMB[15, 21] with the coupling between dark sectors, which is different from the Λ CDM model. Thirdly, the perturbations of the particle distribution are calculated by using 2LPTic[22], which is properly modified to be consistent with our models. Fourthly, the N-body simulation code is also heavily modified for consistency.

Instead of treating the dark energy perturbation as a constant excess of gravity at all scales and redshifts [9, 10], we include the dark energy perturbation self-consistently as a function of scale (k) and redshift (z) by solving perturbation equations from the modified CAMB[15]. We also modify the N-body simulation code Gadget2[23] into ME-Gadget. Technical details can be found in our paper in preparation [19]. We find that ME-Gadget is as efficient as the original Gadget2 code, and the testing results are consistent with [10] by using their models. Our convergence test results also show that our code can reach 5% accuracy as k approaching the Nyquist limit for the nonlinear matter power spectrum at $z = 0$. We would like to emphasize that our N-body simulation pipeline is fully self-consistent, accurate and efficient enough for general phenomenological IDE models. The simulation parameters we use are shown in Tab. II, which were constrained from the combination of Planck 2015, Type Ia supernovae, baryon acoustic oscillations, and the Hubble constant observation datasets (PBSH in short hereafter)[15]. We use a comoving box size of $400h^{-1}\text{Mpc}$ and 256^3 particles in our computa-

TABLE II: Cosmological parameters

Parameter	IDE_I	IDE_II	IDE_III	IDE_IV	Λ CDM
$\Omega_b h^2$	0.02223	0.02224	0.02228	0.02228	0.02225
$\Omega_c h^2$	0.0792	0.1351	0.1216	0.1218	0.1198
$100\theta_{MC}$	1.043	1.04	1.041	1.041	1.04077
τ	0.08204	0.081	0.07728	0.07709	0.079
$\ln(10^{10} A_s)$	3.099	3.097	3.088	3.087	3.094
n_s	0.9645	0.9643	0.9624	0.9624	0.9645
w	-0.9191	-1.088	-1.104	-1.105	-1
ξ_1	—	—	0.0007127	0.000735	—
ξ_2	-0.1107	0.05219	—	0.000735	—
H_0	68.18	68.35	68.91	68.88	67.27
Ω_m	0.2204	0.3384	0.3045	0.3053	0.3156

tions.

MATTER POWER SPECTRUM

The matter power spectrum is used to quantify the large-scale structures. The linear evolution of the matter power spectrum can be simply calculated by linear growth theory. People usually use halofit[11] to estimate the non-linear matter power spectrum at low redshifts. However, since halofit is an empirical fit to Λ CDM N-body simulations, it is not appropriate to use it to describe IDE models. To make it clear, we compare the measured matter power spectrum from our N-body simulations with the prediction of halofit in Fig. 1. The matter power spectrum is computed using the ComputePk code[24]. We find that halofit can marginally be used to describe the nonlinear matter power spectra at $z = 0$ for IDE_III and IDE_IV models, although it is not exactly consistent with that from N-body simulations. This is because the strengths of the interaction in these two models are quite small (~ 0.0007) so that the deviations from the Λ CDM model are negligible. However for models IDE_I and IDE_II, it is clear that halofit cannot give the true matter power spectrum, especially at small scales, because their interactions are relatively large ($|\xi_2| > 0.05$) which cause large deviations from the standard Λ CDM model. The empirical fit to Λ CDM is no longer appropriate in these cases to describe the nonlinear structure, and the appropriate N-body simulations pipeline is called for.

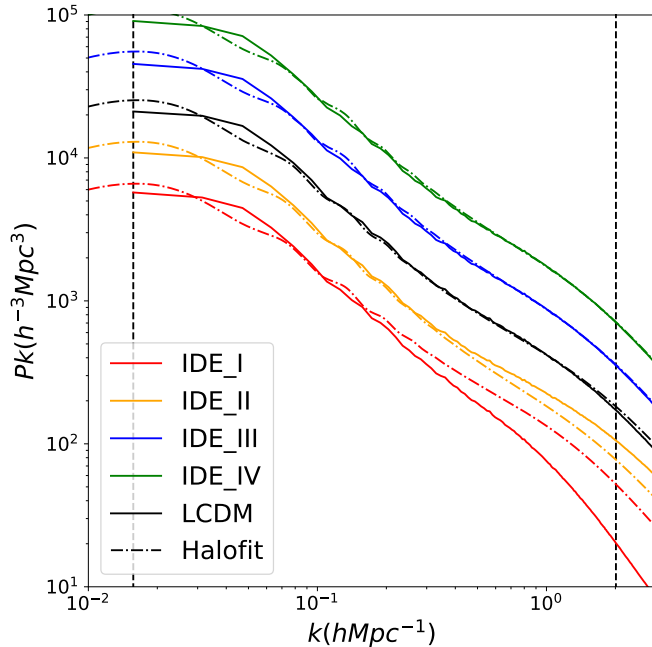


FIG. 1: Different colors show matter power spectra of different models at $z = 0$. Solid lines are measured from N-body simulations while the dash-dotted lines are predicted nonlinear matter power spectra using halofit[11]. We have rescaled IDE.I (IDE.II, IDE.III, IDE.IV) by a factor of $\frac{1}{4}$ ($\frac{1}{2}, 2, 4$) for a better illustration. All the models are identical with Λ CDM (LCDM) at large scales ($k < 0.1 h Mpc^{-1}$). It is clear that halofit is not correct for IDE.I and IDE.II.

GALAXY-GALAXY LENSING

The galaxy images are distorted by the foreground gravitational potential, which is known as gravitational lensing. Assuming an isotropic distribution of both galaxy shape and orientation, any non-zero residual can be considered as such effect, a.k.a. tangential shear γ_T . In galaxy-galaxy lensing, the signal is usually interpreted as the combination of γ_T and the geometry of a lensing system, referring to the critical density $\Sigma_{crit}(z_l, z_s) = \frac{c^2}{4\pi G} \frac{D_s}{D_l D_{ls}}$, where z_l, z_s denote the redshifts of the lens and the source, D_l, D_s and D_{ls} are the angular diameter distances of the lens, source galaxy and the difference between them. The signal measured from galaxy-galaxy lensing actually reflects the differential change of 2D surface density-Excess Surface Density(ESD),

$$\Delta\Sigma(R) = \Sigma(\leq R) - \Sigma(R) = \gamma_t \Sigma_{crit}(z_l, z_s), \quad (4)$$

where $\Sigma(\leq R)$ is the average surface density inside the projected distance R and $\Sigma(R)$ is the surface density at the projected distance R . We use the shear catalog

from[13], which is based on the SDSS DR7 image data. For groups of galaxies we employ the catalog from[25] to identify the lens systems. Following the galaxy-galaxy lensing measurement procedure in[14], we select the most luminous 3660 galaxy groups in the group catalog as the lens in order to be consistent with IDE models. We stack the tangential shear of these 3660 lens systems to measure the ESD. Taking the halos of the same abundance as that in the observation in our N-body simulations, we select the most massive 1771 halos and stack their particles to measure the ESD. The results are shown in Fig. 2. We find that the measured data points are systematically lower than the prediction from the Λ CDM model shown in black dashed line, which is mainly due to the Eddington bias[14]. The Eddington bias comes from the incorrect estimation of the halo mass using the galaxy luminosity or other indicators. The incorrect estimation will mistakenly identify lower mass halos as higher mass halos, thus contaminate the ESD signal. We corrected the Eddington bias by assuming a 0.3 dex incorrect mass estimation following[14], shown as the solid lines. We have tested that the Eddington bias introduced in[14] is similar for IDE models by using the halo catalogs from our simulations. The shaded area represents the redshift bin. The groups of galaxies we selected locate at different redshifts, central at $z = 0.15$ (range $0.01 < z < 0.2$). Thus, the uncertainty due to the redshift difference was also taken into account in our analysis. We estimate the redshift bin by measuring the ESD signal from simulation snapshots at $z = 0.1$ and $z = 0.2$ separately. The solid lines show the central value of the shaded area with the same colors. Even with such conservative treatments, it is still quite clear that IDE.I and IDE.II are not favored by the SDSS galaxy-galaxy weak lensing data, even though these two IDE models are well constrained by PBSH. Therefore, tight constraints from comparing our simulations with observational galaxy-galaxy lensing signals are expected.

CONSTRAINTS

We estimate the constraints from galaxy-galaxy lensing signals by assuming that the ESD signal deviation from the Λ CDM model in logarithmic space is linearly proportional to the interaction strength. We have tested that the above assumption is not significantly affected by the choice of logarithmic space or linear space.

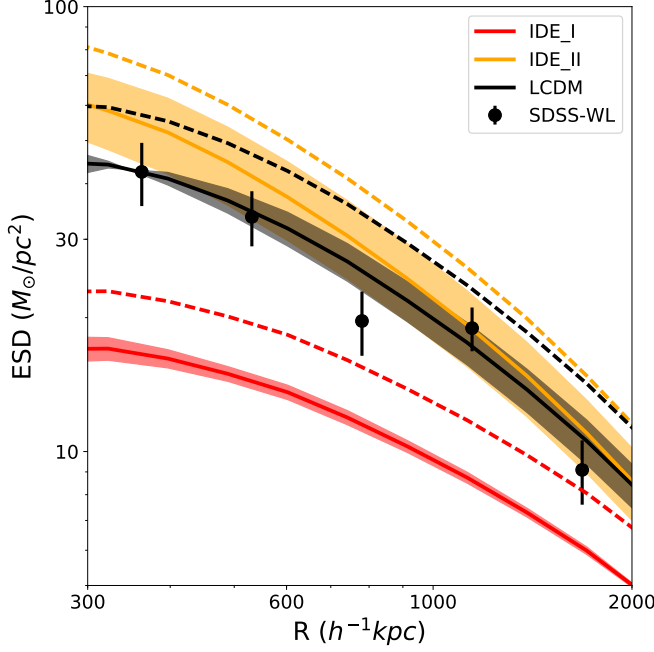


FIG. 2: The Excess Surface Density (ESD) measured from IDE_I, IDE_II and Λ CDM (LCDM) model simulations is shown in red, orange and black respectively. The shaded regions show the ESD range between $z = 0.1$ and $z = 0.2$, which illustrate the redshift uncertainty. The solid (dashed) lines show the results with (without) the Eddington bias corrections. The Λ CDM model is clearly more favored by the SDSS galaxy-galaxy weak lensing data (SDSS-WL) than IDE_I and IDE_II. Because IDE_III and IDE_IV results are almost identical to Λ CDM, we hide them for a better illustration.

The likelihood is constructed as

$$L = \exp(-0.5 * \sum_i \frac{[\Delta\Sigma(R_i)_{sim} - \Delta\Sigma(R_i)_{obs}]^2}{\sigma_z^2 + \sigma_{obs}^2}). \quad (5)$$

Here R_i denotes the measured five data points, $\sigma_z = 0.288$ times the width of the shaded area, representing the uncertainty from the redshift bin, and σ_{obs} is the error estimated from the lensing signal. We show the likelihood from our comparison in Fig. 3. Comparing to the linear constraints given by [15] shown in dashed lines, the constraints from our SDSS galaxy-galaxy weak lensing (SDSS-WL) are clearly tighter for models IDE_I and IDE_II. The improvements of constraints for models IDE_III and IDE_IV are negligible and we do not show here. The joint likelihood of PBSH and SDSS-WL is about 820% tighter than PBSH alone for IDE_I. The best-fitted ξ_2 for IDE_I is $\xi_2 = -0.012$, and the best-fitted ξ_2 for IDE_II becomes $\xi_2 = 0$.

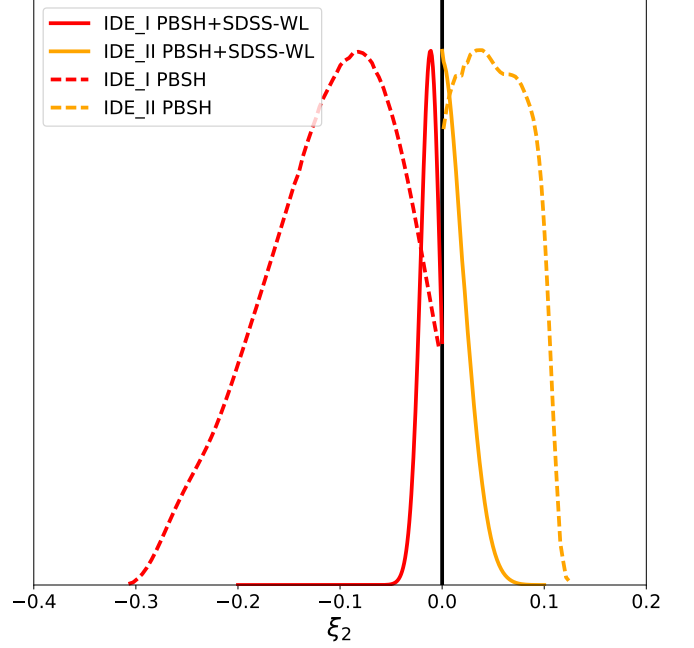


FIG. 3: The constraints of ξ_2 are shown in red (orange) lines for IDE_I (IDE_II). The dashed lines show the constraints from Planck 2015, Baryonic Acoustic Oscillation, Supernovae Type Ia and H0 observations, labelled PBSH in short. The solid lines show the combined constraints from PBSH and SDSS galaxy-galaxy lensing. The improvement for IDE_I and IDE_II is huge. The one sigma lower bound for IDE_I is $\xi_2 = -0.0252$, while the one sigma upper bound for IDE_II is $\xi_2 = 0.0297$. Comparing to PBSH only, the improvement of constraints is $\sim 820\%$ for IDE_I and $\sim 360\%$ for IDE_II.

CONCLUSION

We have successfully devised a self-consistent N-body simulation pipeline to examine the influence of the interaction between dark sectors in structure formation at low redshifts. This formalism is appropriate to general IDE models and efficient in examining the signature of the interaction. With this tool at hand, we do not need to blindly count on halofit, which is an empirical fit to the Λ CDM model, to disclose nonlinear structures.

Considering that interactions in IDE_I and IDE_II models are proportional to the energy density of dark energy, which is sub-dominant at high redshifts, it is natural to find that the constraints of these interactions from PBSH are loose. However with the self-consistent N-body simulation pipeline, we can examine these two models more carefully by using the nonlinear low redshift observations, such as the SDSS galaxy-galaxy weak lensing. It is interesting to find that our first try of the pipeline

can obtain up to 820% improvement of the interaction strength constraint for the IDE.I model. Combining PBSH and SDSS galaxy-galaxy weak lensing measurements, we find the constraint of the interaction strength $\xi_2 = -0.0120^{+0.0120}_{-0.0132}$ for the IDE.I model. For the IDE.II model, combining PBSH and SDSS galaxy-galaxy weak lensing datasets we obtain $\xi_2 = 0.0^{+0.0297}_{-0.0}$, which is also improved significantly by including the nonlinear structure information. For IDE models III and IV, the galaxy-galaxy lensing constraints by employing N-body simulations do not improve much of the constraints if we compare with the linear PBSH results. It is interesting that our pipeline is effective in disclosing physics in the structure formation when there is coupling between dark sectors and it can also help to refine interacting dark energy models by combining with nonlinear structure information.

ACKNOWLEDGEMENT

J.Z acknowledges the support from China Postdoctoral Science Foundation 2018M632097. W.L acknowledges the support from NSFC 11503064 and Shanghai Jiao Tong University and University of Michigan Joint Foundation (AF0720054). The work of B. W was partially supported by NNSFC.

-
- [1] Planck Collaboration, R. Adam, P. A. R. Ade, N. Aghanim, Y. Akrami, M. I. R. Alves, F. Argüeso, M. Arnaud, F. Arroja, M. Ashdown, and et al., **A&A** **594**, A1 (2016), [arXiv:1502.01582](#).
 - [2] S. Perlmutter, G. Aldering, M. della Valle, S. Deustua, R. S. Ellis, S. Fabbro, A. Fruchter, G. Goldhaber, D. E. Groom, I. M. Hook, A. G. Kim, M. Y. Kim, R. A. Knop, C. Lidman, R. G. McMahon, P. Nugent, R. Pain, N. Panagia, C. R. Pennypacker, P. Ruiz-Lapuente, B. Schaefer, and N. Walton, **Nature** **391**, 51 (1998), [astro-ph/9712212](#).
 - [3] A. G. Riess, A. V. Filippenko, P. Challis, A. Clocchiatti, A. Diercks, P. M. Garnavich, R. L. Gilliland, C. J. Hogan, S. Jha, R. P. Kirshner, B. Leibundgut, M. M. Phillips, D. Reiss, B. P. Schmidt, R. A. Schommer, R. C. Smith, J. Spyromilio, C. Stubbs, N. B. Suntzeff, and J. Tonry, **AJ** **116**, 1009 (1998), [astro-ph/9805201](#).
 - [4] S. Perlmutter, G. Aldering, G. Goldhaber, R. A. Knop, P. Nugent, P. G. Castro, S. Deustua, S. Fabbro, A. Goobar, D. E. Groom, I. M. Hook, A. G. Kim, M. Y. Kim, J. C. Lee, N. J. Nunes, R. Pain, C. R. Pennypacker, R. Quimby, C. Lidman, R. S. Ellis, M. Irwin, R. G. McMahon, P. Ruiz-Lapuente, N. Walton, B. Schaefer, B. J. Boyle, A. V. Filippenko, T. Matheson, A. S. Fruchter, N. Panagia, H. J. M. Newberg, W. J. Couch, and T. S. C. Project, **ApJ** **517**, 565 (1999), [astro-ph/9812133](#).
 - [5] K. G. Begeman, A. H. Broeils, and R. H. Sanders, **MNRAS** **249**, 523 (1991).
 - [6] M. Persic, P. Salucci, and F. Stel, **MNRAS** **281**, 27 (1996), [astro-ph/9506004](#).
 - [7] L. Chemin, W. J. G. de Blok, and G. A. Mamon, **AJ** **142**, 109 (2011), [arXiv:1109.4247 \[astro-ph.CO\]](#).
 - [8] B. Wang, E. Abdalla, F. Atrio-Barandela, and D. Pavón, **Reports on Progress in Physics** **79**, 096901 (2016), [arXiv:1603.08299](#).
 - [9] M. Baldi, V. Pettorino, G. Robbers, and V. Springel, **MNRAS** **403**, 1684 (2010), [arXiv:0812.3901](#).
 - [10] M. Baldi, **MNRAS** **414**, 116 (2011), [arXiv:1012.0002](#).
 - [11] R. Takahashi, M. Sato, T. Nishimichi, A. Taruya, and M. Oguri, **ApJ** **761**, 152 (2012), [arXiv:1208.2701](#).
 - [12] R. An, C. Feng, and B. Wang, **JCAP** **2**, 038 (2018), [arXiv:1711.06799](#).
 - [13] W. Luo, X. Yang, J. Zhang, D. Tweed, L. Fu, H. J. Mo, F. C. van den Bosch, C. Shu, R. Li, N. Li, X. Liu, C. Pan, Y. Wang, and M. Radovich, **ApJ** **836**, 38 (2017), [arXiv:1607.05406](#).
 - [14] W. Luo, X. Yang, T. Lu, F. Shi, J. Zhang, H. J. Mo, C. Shu, L. Fu, M. Radovich, J. Zhang, N. Li, T. Sunayama, and L. Wang, **ArXiv e-prints** (2017), [arXiv:1712.09030](#).
 - [15] A. A. Costa, X.-D. Xu, B. Wang, and E. Abdalla, **JCAP** **1**, 028 (2017), [arXiv:1605.04138](#).
 - [16] M. Baldi, **MNRAS** **411**, 1077 (2011), [arXiv:1005.2188](#).
 - [17] J.-H. He, B. Wang, and E. Abdalla, **Physics Letters B** **671**, 139 (2009), [arXiv:0807.3471 \[gr-qc\]](#).
 - [18] J.-H. He, B. Wang, and Y. P. Jing, **JCAP** **7**, 030 (2009), [arXiv:0902.0660 \[gr-qc\]](#).
 - [19] J. Zhang, in preperation (2018).
 - [20] S. Liao, **ArXiv e-prints** (2018), [arXiv:1807.03574](#).
 - [21] A. Lewis and A. Challinor, “CAMB: Code for Anisotropies in the Microwave Background,” **Astrophysics Source Code Library** (2011), [ascl:1102.026](#).
 - [22] M. Crocce, S. Pueblas, and R. Scoccimarro, **MNRAS** **373**, 369 (2006), [astro-ph/0606505](#).
 - [23] V. Springel, **MNRAS** **364**, 1105 (2005), [astro-ph/0505010](#).
 - [24] B. L’Huillier, “computePk: Power spectrum computation,” **Astrophysics Source Code Library** (2014), [ascl:1403.015](#).
 - [25] X. Yang, H. J. Mo, F. C. van den Bosch, A. Pasquali, C. Li, and M. Barden, **ApJ** **671**, 153 (2007), [arXiv:0707.4640](#).